



# Effect of calcination temperature on carbon dioxide separation properties of a novel microporous hybrid silica membrane

Hong Qi\*, Jing Han, Nanping Xu

State Key Laboratory of Materials-Oriented Chemical Engineering, Membrane Science and Technology Research Center, Nanjing University of Technology, Nanjing 210009, China

## ARTICLE INFO

### Article history:

Received 20 April 2011

Received in revised form 25 July 2011

Accepted 8 August 2011

Available online 16 August 2011

### Keywords:

CO<sub>2</sub> separation

Hybrid silica membranes

1,2-Bis(triethoxysilyl)ethane

Niobium penta(n)butoxide

Calcination temperature

## ABSTRACT

A novel microporous hybrid silica membrane for the separation of carbon dioxide, fabricated through sol-gel deposition of a microporous Nb-doped ethylene-bridged silsesquioxane layer on a multilayer porous support, was reported. Effect of the calcination temperature on H<sub>2</sub>/CO<sub>2</sub> separation properties of Nb-BTESE membrane was investigated. Low CO<sub>2</sub> permeance was imparted by doping acidic niobium centers into the hybrid silica networks. Denser hybrid silica networks as well as more Lewis acid sites were generated as the calcination temperature elevated, which imparted very low CO<sub>2</sub> permeance to the novel hybrid membrane while retaining its relative high H<sub>2</sub> flux in the order of  $\sim 10^{-7}$  mol m<sup>-2</sup> s<sup>-1</sup> Pa<sup>-1</sup>. Dominant densification occurred in the Nb-doped hybrid silica networks when the calcination temperature was lower than 400 °C. Meanwhile, the Nb-BTESE membrane showed relatively weak acidity which was induced by niobium doping. Dual effects are working when the heat-treated temperature was higher than 400 °C. On the one hand, the increased surface acidity reduced the number of sites and/or affinity for adsorption of CO<sub>2</sub> as the calcination temperature elevated. On the other hand, membrane densification occurred during the calcination process. Therefore, the permselectivity of H<sub>2</sub>/CO<sub>2</sub> for Nb-BTESE membrane could be tuned by altering the calcination temperature. The Nb-BTESE membrane calcined at 450 °C showed both relative high hydrogen permeance ( $\sim 9.7 \times 10^{-8}$  mol m<sup>-2</sup> s<sup>-1</sup> Pa<sup>-1</sup>) and excellent H<sub>2</sub>/CO<sub>2</sub> permselectivity (220), as compared with Nb-BTESE membranes calcined at other temperatures.

© 2011 Elsevier B.V. All rights reserved.

## 1. Introduction

Inorganic membrane technology for the separation of gases is foreseen to play an important role in reducing the environmental impact and costs of many industrial processes. Several materials have been proposed to be used as molecular sieving membranes, including zeolites, carbon, silica and metal oxides. These generally consist of a thin separation layer with thickness between a few tens nanometers up to a few microns superimposed on a mechanically strong porous support. Supported membranes prepared from amorphous silica with pore sizes (2–5 Å) tailored to the kinetic diameter of the gas phase molecule of interest have received major attention due to their high performance, i.e., flux and selectivity, at elevated temperatures [1–6]. However, the modest stability of amorphous silica under humid conditions severely limits its application in many industrial processes. To improve the hydrothermal stability of silica membranes, modification of silica with metal oxides [7–13] or hydrophobic silanes [14,15] have been put forward as alternative approaches, which can be found in Table 1.

Those modified silica membranes do exhibit higher stability in the presence of hot steam, in comparison with that of pure silica membranes. However, if we pay attention to the separation property with respect to H<sub>2</sub>/CO<sub>2</sub> (or He/CO<sub>2</sub>), we can find that H<sub>2</sub> (or He) permeances of those modified silica membranes were normally in the range of  $\sim 10^{-8}$  to  $\sim 10^{-7}$  mol m<sup>-2</sup> s<sup>-1</sup> Pa<sup>-1</sup>. Although a H<sub>2</sub> permeance as high as  $4.24 \times 10^{-6}$  mol m<sup>-2</sup> s<sup>-1</sup> Pa<sup>-1</sup> [15] can be obtained, the H<sub>2</sub>/CO<sub>2</sub> permselectivity for fluorocarbon-modified silica membrane was only 11, which is only a bit higher than Knudsen value. Battersby et al. [9] reported that the Co-doped silica membrane provided with an increased H<sub>2</sub>/CO<sub>2</sub> permselectivity, measured in their study as high as 1000. However, much lower H<sub>2</sub> permeance of  $6 \times 10^{-9}$  mol m<sup>-2</sup> s<sup>-1</sup> Pa<sup>-1</sup> was observed.

Recently, a promising He/CO<sub>2</sub> separation membrane was fabricated through sol-gel approach, by using 1,2-bis(triethoxysilyl)ethane (BTESE) and niobium penta(n)butoxide as precursors [16]. Results showed that not only high helium permeance and low CO<sub>2</sub> flux can be obtained, but also the membrane retained its permselectivity as high as 3700 towards He/CO<sub>2</sub> in the presence of hot steam, indicating a superior hydrothermal stability required to be applicable to industrially relevant gas steams. It is well known that properties of microporous membranes are determined by many factors, such as polymeric sol structure,

\* Corresponding author. Tel.: +86 25 83172279; fax: +86 25 83172292.

E-mail addresses: [hqinjut@yahoo.com.cn](mailto:hqinjut@yahoo.com.cn), [hqi@njut.edu.cn](mailto:hqi@njut.edu.cn) (H. Qi).

**Table 1**  
Progresses regarding the microporous modified silica membranes for gas separation in recent 3 years.

Fabrication route	Support/configuration	Membrane materials	Membrane thickness/nm	Gas components (A/B)	Permeance $P_A/(\text{mol m}^{-2} \text{s}^{-1} \text{Pa}^{-1})$	Test temperature/ $^{\circ}\text{C}$	Permselectivity/ $F_{\alpha}$	Reference	
Sol-Gel	$\gamma\text{-Al}_2\text{O}_3$ /platelet	Co-SiO <sub>2</sub>	150	He/N <sub>2</sub>	$\sim 9.5 \times 10^{-8}$	160	350	[7]	
Sol-Gel	$\gamma\text{-Al}_2\text{O}_3$ /disk	Nb-SiO <sub>2</sub>		H <sub>2</sub> /CO <sub>2</sub>	$4.0 \times 10^{-8}$	200	43.2	7.0	[8]
Sol-Gel	$\gamma\text{-Al}_2\text{O}_3$ /tubular	Co-SiO <sub>2</sub>	250	He/N <sub>2</sub>	$5.0 \times 10^{-9}$	250	4800	1000	
CVD	$\gamma\text{-Al}_2\text{O}_3$ /tubular	Al <sub>2</sub> O <sub>3</sub> -SiO <sub>2</sub>	30–40	H <sub>2</sub> /CO <sub>2</sub>	$3.0 \times 10^{-8}$				
				H <sub>2</sub> /CH <sub>4</sub>	$6.0 \times 10^{-9}$	600	940	700	590
				H <sub>2</sub> /CO	$2.0\text{--}3.0 \times 10^{-7}$				
Sol-Gel	SiO <sub>2</sub> -ZrO <sub>2</sub> /tubular	Pd-SiO <sub>2</sub>	100–200	H <sub>2</sub> /CO <sub>2</sub>	$3.0 \times 10^{-7}$	500	150	<10	[11]
Sol-Gel	SiO <sub>2</sub> -ZrO <sub>2</sub> /tubular	Me-SiO <sub>2</sub> (M = Co, Ni, Fe, Al)		H <sub>2</sub> /N <sub>2</sub>	$4.5 \times 10^{-7}$	500	>100		[12]
Sol-Gel	SiO <sub>2</sub> -ZrO <sub>2</sub> /tubular	Ni-SiO <sub>2</sub>	200	He/N <sub>2</sub>	$7.2 \times 10^{-7}$	500	1450		[12]
Sol-Gel	$\gamma\text{-Al}_2\text{O}_3$ /tubular	B <sub>2</sub> O <sub>3</sub> -SiO <sub>2</sub>		He/CO <sub>2</sub>	$\sim 10^{-7}$	300	55		[13]
Sol-Gel	SiO <sub>2</sub> -ZrO <sub>2</sub> /tubular	Hybrid SiO <sub>2</sub>	40	H <sub>2</sub> /N <sub>2</sub>	$8.27 \times 10^{-6}$	200	8.97	1050	[14]
				H <sub>2</sub> /SF <sub>6</sub>					
Sol-Gel	$\gamma\text{-Al}_2\text{O}_3$ /disk	Fluorocarbon-modified SiO <sub>2</sub>		H <sub>2</sub> /CO <sub>2</sub>	$4.24 \times 10^{-6}$	250	11	47	[15]
				H <sub>2</sub> /SF <sub>6</sub>					

dip-coating parameters and heat-treated conditions. Taking into account that the calcination temperature of 450 °C is close to the decomposition of the bridging groups ( $\sim 470$  °C) reported by literature [14], and more important, calcination temperature plays a key role on the surface acidity of catalysts [17–19], more information regarding the effect of calcination temperature on properties of Nb-doped hybrid silica membrane, especially on gas separation behavior, is needed. In this paper, we report the micro-structural characteristics and gas permeation properties of disk Nb-BTESE membranes calcined at different temperatures.

## 2. Experimental

### 2.1. Fabrication of polymeric sol and hybrid silica membranes

Niobium-doped hybrid silica sol was prepared by using 1,2-bis(triethoxysilyl)ethane ((C<sub>2</sub>H<sub>5</sub>O)<sub>3</sub>Si-CH<sub>2</sub>-CH<sub>2</sub>-Si(C<sub>2</sub>H<sub>5</sub>O)<sub>3</sub>, BTESE, purity 97%, ABCR) and niobium penta(n)butoxide (NPB, purity 99%, ABCR) as precursors. 5 ml BTESE was added to 5 ml absolute ethanol (dried, Secco Solv, max. 0.02% H<sub>2</sub>O, Merck) in nitrogen glove-box. 0.54 ml of nitric acid was drop-wise added into the BTESE solution under vigorous stirring. The mixture was then reflux at 60 °C in water bath for 90 min. Subsequently, 3.75 ml of NPB dissolved in 13 ml absolute ethanol, together with another 0.54 ml of nitric acid, were drop-wise introduced into the above-mentioned sol with mol ratio for Si:Nb was 3:1. The refluxing was maintained at 60 °C for an additional 90 min with the final mol ratio of sol for BTESE:NPB:ethanol:HNO<sub>3</sub>:H<sub>2</sub>O was 1:0.33:6.3:0.08:4.45. The polymeric hybrid silica sol was cooled down to the room temperature and diluted for 6 times with ethanol before dip-coating. Supported membranes were fabricated through dip-coating the above-mentioned sol onto home-made disk  $\alpha$ -alumina supported mesoporous  $\gamma$ -alumina layer under clean room (class 1000) conditions. After that, the Nb-BTESE membranes were calcined under dry nitrogen in the temperature range of 300–500 °C for 3 h (hereafter referred to as Nb-BTESE 300, Nb-BTESE 350, Nb-BTESE 400, Nb-BTESE 450 and Nb-BTESE 500, respectively), with the heating and cooling rates of both 0.5 °C min<sup>-1</sup>. Nb-BTESE powders were obtained by drying corresponding hybrid silica sol in a Petri dish overnight, followed by calcination procedures which are the same as that found for supported membranes.

### 2.2. Characterization

The phase compositions of dried gel powders, as well as powders heat-treated at different temperatures, were probed by X-ray diffraction (XRD, Bruker D8 Advance diffractometer) with Cu K $\alpha$  radiation. Fourier transform infrared (FT-IR) spectroscopy was performed both on dried and on calcined powders at room temperature in a wave-number region from 4000 to 400 cm<sup>-1</sup> on a Tensor 27 FT-IR spectrometer (Bruker Optics), using a transmission cell and KBr as reference. Gas adsorption measurements were conducted at 77 K (N<sub>2</sub>) and 298 K (CO<sub>2</sub>), respectively, both on ASAP 2020 (Micromeritics) instruments. Prior to measurements, all samples were degassed under vacuum at 300 °C for 48 h. Temperature programmed desorption (TPD, TP5080, Xianquan Co. Ltd. Tianjin, China) technique was used to evaluate the acidity of the Nb-BTESE powders heat-treated at different temperatures. 40 mg of powder was pre-treated in helium (flow rate: 35.5 ml/min) at 300 °C for 1 h prior to ammonia adsorption, which was carried out at 100 °C for 1 h. Helium was subsequently introduced once again till the baseline was stable. After that, the system reached a temperature of 900 °C at a heating rate of 10 °C min<sup>-1</sup>, under which desorption process occurred. NH<sub>3</sub>-TPD signals were detected

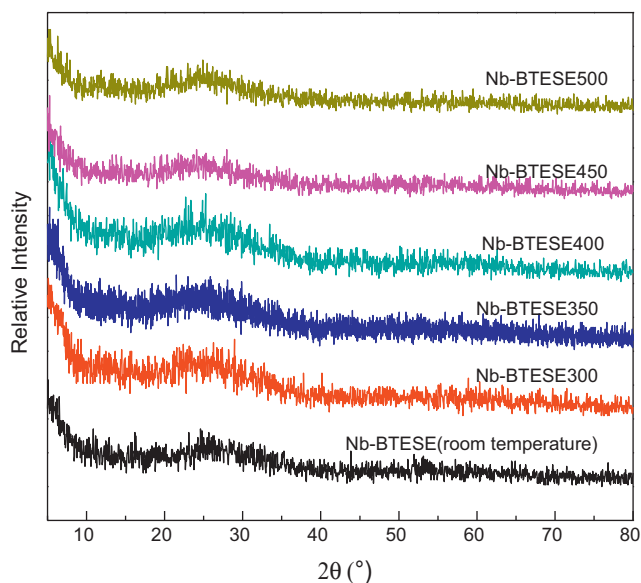


**Fig. 1.** XRD patterns of Nb-BTESE powders calcined in nitrogen at different temperatures. Also shown are data for Nb-BTESE gel powders dried at room temperature.

with TCD detector. X-ray photoelectron spectroscopy (XPS) measurements were performed on a PHI 5000 VersaProbe equipped with a monochromatic Al K $\alpha$  X-ray source (1486.6 eV). The binding energies (BE) of O 1s were determined by computer fitting the measured spectra and were referenced to the C 1s peak of the adventitious carbon (283.8 eV). Single gas permeation measurements were conducted in a dead-end mode set-up. The pressure difference across the membrane was 0.3 MPa, while the permeate side was vented to the atmosphere. The gas flow rate was measured with a soap-film flow meter. Gas permeances of hybrid silica membranes were measured in a sequence starting with the smallest kinetic diameter, from He (0.255 nm), H<sub>2</sub> (0.289 nm), CO<sub>2</sub> (0.33 nm), O<sub>2</sub> (0.346 nm), N<sub>2</sub> (0.365 nm), CH<sub>4</sub> (0.382 nm) to SF<sub>6</sub> (0.55 nm). All gas permeances were measured at 200 °C and 0.3 MPa.

### 3. Results and discussion

#### 3.1. Characterization of dried gel powders

X-ray diffraction (XRD) patterns of Nb-BTESE powders dried at room temperature (25 °C) as well as thermally treated in the range of 300–500 °C, are given in Fig. 1. Fig. 2 presents XRD patterns of micrometer-sized Nb<sub>2</sub>O<sub>5</sub> powders and a simple mixture of BTESE with micrometer-sized Nb<sub>2</sub>O<sub>5</sub> powders. For comparison, also shown in Fig. 2 are XRD patterns of BTESE powders as well as Nb-BTESE powders, both dried at room temperature. The absence of any Bragg reflections in the powder XRD patterns shown in Fig. 1 indicated the formation of amorphous phases, which are well dispersed on hybrid silica. However, it cannot be excluded that the niobium composites had crystallite sizes smaller than the detection limit for Cu-K $\alpha$  radiation, as proposed by Francisco and Gushikem [20], and Pereira et al. [21]. Francisco and Gushikem [20] reported that no crystallization form is found for niobium-doped silica powder with Nb loading amount in the range of 2.5–7.5% when the calcination temperature was lower than 800 °C. Crystallization of Nb<sub>2</sub>O<sub>5</sub> can be detected after thermal treatment above 1000 °C, depending on loading amount.

Fourier transform infrared (FT-IR) spectroscopy was employed to monitor the incorporation of Nb into the ethylene-bridged polysilsesquioxane networks and to study the calcination behav-

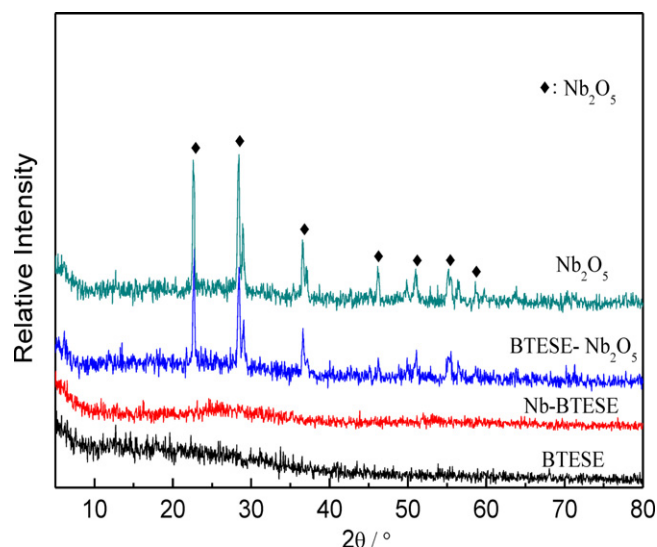


**Fig. 2.** XRD patterns of Nb-BTESE, BTESE, BTESE-Nb<sub>2</sub>O<sub>5</sub> and Nb<sub>2</sub>O<sub>5</sub> powders. All the powders are dried at room temperature.

ior. Fig. 3 recorded FT-IR spectra of Nb-BTESE powders calcined at 300 °C, 350 °C, 450 °C and 500 °C (denoted as Nb-BTESE 300, Nb-BTESE 350, Nb-BTESE 450 and Nb-BTESE 500), respectively. One of the pronounced features in Fig. 3, is the intensity of Si-OH stretching vibration at 3410–3430 cm<sup>-1</sup> diminished apparently as the calcination temperature increased. It may be the case that silanol groups were consumed by further condensation to form more densified silica structures during heat treatment. The characteristic absorption bands at 2870–2980 cm<sup>-1</sup> for the sp<sup>3</sup> C-H stretching vibrations [22,23], together with CH<sub>2</sub> vibrations at ~1270 cm<sup>-1</sup> and ~1410 cm<sup>-1</sup> [24,25] can be regarded as evidences for the presence of Si-CH<sub>2</sub>-CH<sub>2</sub>-Si in those powders. It should be noted, however, that intensities of those peaks decreased with calcination temperature, and tended to disappear at a calcination temperature of 500 °C. This result lines up with our previous TG/DTA observation [16] for Nb-BTESE powders, showing partial pyrolysis occurs at an onset temperature of ca. 470 °C. Peaks at about 1678 cm<sup>-1</sup> was due to the deformation of water molecular,

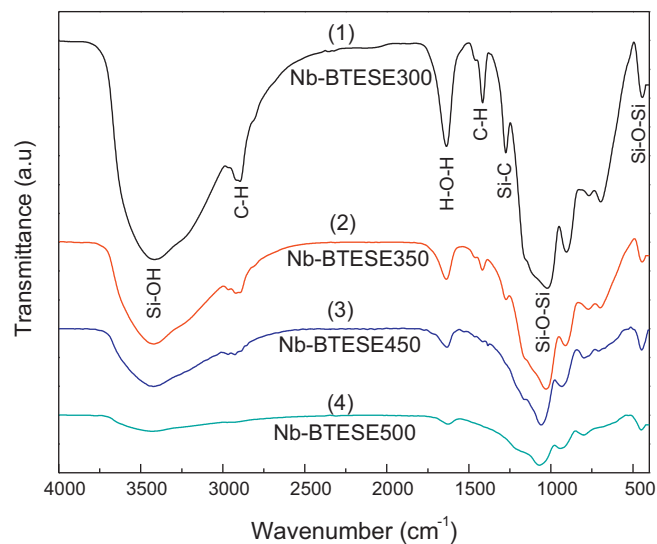


**Fig. 3.** FT-IR spectra of Nb-BTESE gel powders calcined under nitrogen at (1): 300 °C, (2): 350 °C, (3): 450 °C and (4): 500 °C, respectively (denoted as Nb-BTESE 300, Nb-BTESE 350, Nb-BTESE 450, Nb-BTESE 500).

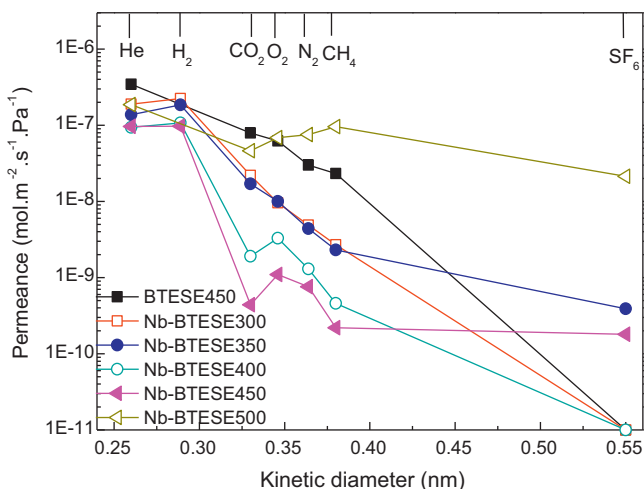


**Fig. 4.** Single gas permeances of BTESE membrane (calcined at 450 °C) and Nb-BTESE membranes (calcined in the range of 300–500 °C) as a function of kinetic diameter of the permeating gas molecule measured at 200 °C and 0.3 MPa.

and the amplitude tended to reduce with the calcination temperature. Stretching vibrations at around 1000–1100  $\text{cm}^{-1}$  [26] were caused by Si–O–Si and obvious shifting can be found from 1022  $\text{cm}^{-1}$  (for Nb-BTESE 300), 1059  $\text{cm}^{-1}$  (for Nb-BTESE 450) to 1070  $\text{cm}^{-1}$  (for Nb-BTESE 500). Results of infrared absorption bands for Si–OH and Si–O–Si networks varied with thermal treatment conditions, are agreed with the data reported in literature [27,28].

### 3.2. Gas permeances properties of Nb-BTESE membranes and its $\text{H}_2/\text{CO}_2$ separation mechanism

Single gas permeances of BTESE membrane (calcined at 450 °C) and Nb-BTESE membranes (calcined in the range of 300–500 °C) as a function of kinetic diameter of the permeating gas molecule, measured at 200 °C and 0.3 MPa, are displayed in Fig. 4. As can be seen in Fig. 4, BTESE 450 membrane showed high helium permeance of  $3.45 \times 10^{-7} \text{ mol m}^{-2} \text{ s}^{-1} \text{ Pa}^{-1}$  with  $\text{He}/\text{CO}_2$  permselectivity of 4.4, which is similar to the corresponding Knudsen value (3.3). Nb-BTESE 300 membrane, although calcined at 300 °C, exhibited helium permeance of  $1.89 \times 10^{-7} \text{ mol m}^{-2} \text{ s}^{-1} \text{ Pa}^{-1}$  while maintained similar variation tendency if compared with that of the BTESE 450 membrane. Additionally, single gas ( $\text{H}_2$ ,  $\text{CO}_2$ ,  $\text{O}_2$ ,  $\text{N}_2$  and  $\text{CH}_4$ ) permeances of Nb-BTESE 450 membrane were one order of magnitude lower than that of BTESE 450 membrane, with He permeance and  $\text{He}/\text{CO}_2$  permselectivity of Nb-BTESE 450 membrane being  $9.68 \times 10^{-8} \text{ mol m}^{-2} \text{ s}^{-1} \text{ Pa}^{-1}$  and 220, respectively. The result confirms that the incorporation of niobium into the hybrid silica networks leads to a more densified membrane structure, like Nb-modified silica membranes, as reported by Boffa et al. [8]. Nb-BTESE 350 membrane, with helium permeance of  $1.38 \times 10^{-7} \text{ mol m}^{-2} \text{ s}^{-1} \text{ Pa}^{-1}$ , showed almost the same gas permeances (except for  $\text{SF}_6$ ) as that found for Nb-BTESE 300 membrane, indicating a higher calcination temperature of 350 °C did not alter the membrane structures too much. If we compare gas permeances of Nb-BTESE 400 membrane with that of Nb-BTESE 450 membrane, we can find that the higher of the calcination temperature, the lower of the corresponding gas permeances. The result is reasonable since a higher temperature could lead to a much more dense membrane structure.

It should be noted in Fig. 4 that hydrogen permeance of Nb-BTESE membrane is always higher than that of helium, regardless of calcination temperature. Kanezashi et al. [29] proposed that microporous silica membranes, prepared by sol–gel method,

consist of interparticle pores and intraparticle pores. The interparticle pores are formed by spaces between gel particles, while silica network structure provides the intraparticle pores. Hydrogen and helium, with relative small kinetic diameter, can permeate through both types of pores. Gases with larger size, such as  $\text{N}_2$  and  $\text{SF}_6$ , can flow through only the interparticle pores formed by spaces between gel particles, which are believed to be much larger than intraparticle pores. The transport mechanisms for gases permeate through interparticle pores and intraparticle pores are molecular sieving (governed by activated diffusion) and Knudsen diffusion, respectively. With respect to hydrogen and helium transport through Nb-BTESE membranes fabricated in this study, the governed mechanism should be activated diffusion if taken account of the membrane permselectivities regarding  $\text{H}_2/\text{CO}_2$  (or  $\text{He}/\text{CO}_2$ ), which are all well above Knudsen values. Ikuhara et al. [30] observed that  $\text{H}_2$  permeance of Ni-doped silica membrane is approximately five times higher than that of helium. They ascribed the result to the reversibly adsorbed hydrogen property of Ni-doped amorphous silica materials, which resulted in increased number of solubility sites for hydrogen and hence improved hydrogen permeance. It might be the case that enhanced hydrogen adsorption led to increased  $\text{H}_2$  permeance of Nb-BTESE membranes, as a result of incorporating Nb into hybrid silica matrix.

Table 2 shows  $\text{H}_2/\text{CO}_2$  and  $(\text{He})/\text{CO}_2$  permselectivities of Nb-BTESE membranes calcined at various temperatures. The  $\text{H}_2/\text{CO}_2$  permselectivity increased remarkably with the calcination temperature, from 10.2 (Nb-BTESE 300) to 220 (Nb-BTESE 450), which could be assigned to the fact that the  $\text{CO}_2$  permeance declined appreciably from  $2.2 \times 10^{-8} \text{ mol m}^{-2} \text{ s}^{-1} \text{ Pa}^{-1}$  (Nb-BTESE 300) to  $4.4 \times 10^{-10} \text{ mol m}^{-2} \text{ s}^{-1} \text{ Pa}^{-1}$  (Nb-BTESE 450) as the calcination temperature elevated. Meanwhile,  $\text{H}_2$  permeance of Nb-BTESE membrane maintained at a relative high value of  $1-2 \times 10^{-7} \text{ mol m}^{-2} \text{ s}^{-1} \text{ Pa}^{-1}$ . This phenomenon indicated that the gradually advanced calcination temperature reduced  $\text{CO}_2$  permeance by the membrane structure densification. de Vos and Verweij [1] also observed a large increasing of permselectivity for  $\text{H}_2/\text{CO}_2$  from 7 (for Si-400 membrane) to ca. 70 (for Si-600 membrane). On the one hand, the higher calcination temperature leads to densification of silica membrane structures and a smaller pore size. On the other hand, the reduced amount of hydroxyls makes the material more hydrophobic, resulting in a lower (surface) occupation and hence, a lower  $\text{CO}_2$  permeance. Therefore, the permselectivity of  $\text{H}_2/\text{CO}_2$  and  $(\text{He})/\text{CO}_2$  for Nb-BTESE membrane could be tuned by altering the calcination temperature. However, it should be noted that gas permeances of the small molecules, such as helium and hydrogen, did not vary too much, and maintained at about  $1-3 \times 10^{-7} \text{ mol m}^{-2} \text{ s}^{-1} \text{ Pa}^{-1}$ . With respect to Nb-BTESE membrane calcined at 500 °C, it lost molecular sieving properties and Knudsen diffusion was the dominant mechanism. This can be ascribed to the breakage of the  $-\text{Si}-\text{CH}_2-\text{CH}_2-\text{Si}-$  structure due to a much higher calcination temperature, as evidenced by TG-DTA curves [16]. Most to our surprise, however, was that  $\text{CO}_2$  transportation through Nb-BTESE 400 and Nb-BTESE 450 membranes showed an irregular tendency as that found for other gases, which should demonstrate a reduced gas permeance with increasing of kinetic diameter of the gas. We [16] have proposed recently that the altered density and strength of the acidic surface centers of hybrid silica membranes might be imparted by niobium incorporation, and subsequently resulted in a much lower  $\text{CO}_2$  permeance. To confirm the hypothesis,  $\text{CO}_2$  adsorption isotherms of Nb-doped hybrid silica powders that heat-treated at various temperatures were measured at 298 K and the result, as compared with that of BTESE 450, are given in Fig. 5. As can be observed in Fig. 5,  $\text{CO}_2$  adsorption capacity of Nb-BTESE powder decreased as the calcination temperature increased. By comparison  $\text{CO}_2$  adsorption capacity of Nb-BTESE powders with that of BTESE 450 powders,

**Table 2**  
H<sub>2</sub>/CO<sub>2</sub> and He/CO<sub>2</sub> permselectivities of Nb–BTESE membranes calcined at different temperatures in the range of 300–500 °C.

Membranes	Calcination temperature <i>T</i> /°C	Gas permeance × 10 <sup>-8</sup> mol m <sup>-2</sup> s <sup>-1</sup> Pa <sup>-1</sup>			Permselectivity	
		He	H <sub>2</sub>	CO <sub>2</sub>	He/CO <sub>2</sub>	H <sub>2</sub> /CO <sub>2</sub>
Nb–BTESE	300	18.9	22.5	2.2	8.6	10.2
	350	13.8	18.5	1.7	8.1	10.9
	400	9.4	10.7	0.19	49	56.3
	450	9.7	9.7	0.044	220	220
	500	18.6	–	4.61	4.0	–

we can find that 300 °C or 350 °C heat-treated Nb–BTESE powders showed similar, even higher CO<sub>2</sub> sorption capacity than that found for BTESE 450 powders. However, Nb–BTESE 400, especially for Nb–BTESE 450 and Nb–BTESE 500 powders, exhibited lower CO<sub>2</sub> sorption volume than that of BTESE 450 powders, showing either the strength of the acidity and/or density of acidic sites of the powders might increased, or more densified membrane structures was formed with the calcination temperature. To clarify the effect of calcination temperature on Nb–BTESE membrane structures, effective surface areas of Nb–BTESE powders were calculated with the Dubinin method [31] based on the CO<sub>2</sub> adsorption isotherm data shown in Fig. 5, as represented with Eq. (1).

$$\log n = \log n_m + D \left( \log \frac{p^0}{p} \right)^2 \quad (1)$$

Subsequently, effective surface areas *A* can be calculated according to Eq. (2).

$$A = n_m a_m N_A \quad (2)$$

where *n* is the gas adsorbed at relative pressure *p*<sup>0</sup>/*p*. *n<sub>m</sub>* is the monolayer adsorption capacity of the surface (mol/g adsorbent). *D* is an adsorbate-dependent constant. *N<sub>A</sub>* is Avogadro's number and *a<sub>m</sub>* is the area occupied by a molecule in the completed monolayer. Based on Eq. (1), *log n* is directly proportional to (log(*p*<sup>0</sup>/*p*))<sup>2</sup>. Effective surface area as well as parameter *D*, *log n<sub>m</sub>*, can be calculated by Eqs. (1) and (2), with the results presented in Table 3. As shown in Table 3, effective surface area reduced with the calcination temperature from 119 m<sup>2</sup>/g (for Nb–BTESE 300) to 26.8 m<sup>2</sup>/g (for Nb–BTESE 450), down by 77.5%. It should be noted, however, that the reduction of effective surface area was not proportional to the increment of temperature (surface area maintained almost

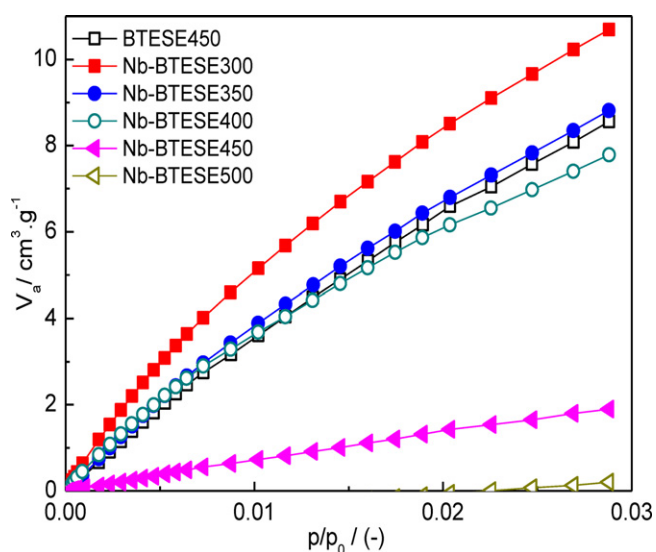


**Fig. 5.** CO<sub>2</sub> adsorption isotherms at 298 K for Nb–BTESE powders calcined in the range of 300–500 °C, as compared with that of BTESE powders calcined at 450 °C.

**Table 3**  
Surface areas, absolute values of the parameter *D* and *log n<sub>m</sub>* calculated from Eqs. (1) and (2).

Powders	CO <sub>2</sub> surface area <i>A</i> , m <sup>2</sup> /g	<i>D</i>   (CO <sub>2</sub> )	<i>log n<sub>m</sub></i>
BTESE 300 [27]	422	0.176	–
BTESE 450	120	0.206	–2.96
Nb–BTESE 300	119	0.170	–2.96
Nb–BTESE 350	126	0.206	–2.93
Nb–BTESE 400	88.4	0.173	–3.09
Nb–BTESE 450	26.8	0.217	–3.61

the same in the range of 300–350 °C, while decreased 29.8% from 350 °C to 400 °C and 70% from 400 °C to 450 °C, respectively). The above-mentioned results, i.e., reduced CO<sub>2</sub> sorption data and effective surface areas with calcination temperature, might be ascribed to either densification of the membrane structures or increased acidity of the powders (including density of acidic sites), or both. However, in the temperature range of 300–450 °C, if we compare the reduction amplitude of CO<sub>2</sub> permeance with that of O<sub>2</sub>, N<sub>2</sub> or CH<sub>4</sub>, as shown in Fig. 4, acidity of the Nb–BTESE membrane with the calcination temperature cannot be neglected.

To ensure that the acidity of the powder plays a causal role on its CO<sub>2</sub> adsorption capacities, NH<sub>3</sub>-TPD test was conducted on Nb–BTESE powders with the results shown in Fig. 6. As can be seen in Fig. 6, two signals at temperatures in the range of ~144 °C and 576–618 °C can be clearly distinguished in TPD spectra, which are corresponding to weak and strong acid sites in Nb–BTESE powder, respectively. Nb–BTESE powders exhibited stronger acidity as the calcination temperature elevated from 300 °C to 450 °C, which can be confirmed with the fact that ammonia desorption temperature increased from 576 °C to 617 °C, respectively. Meanwhile, enlargement for intensity of the corresponding peaks was another evidence, indicating stronger acidity of powder. It should

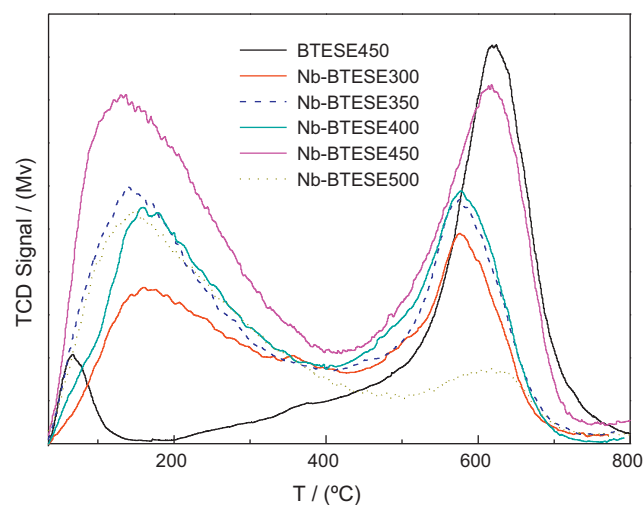


**Fig. 6.** NH<sub>3</sub> temperature programmed desorption (NH<sub>3</sub>-TPD) curves of BTESE 450 powder and Nb–BTESE powders calcined in the temperature range of 300–500 °C.

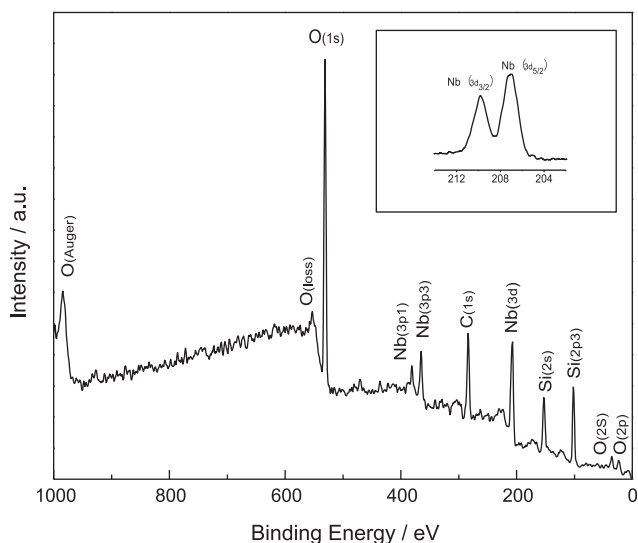


**Fig. 7.** XPS spectrum of Nb-BTESE powder. Also shown inset is the spectrum showing the Nb(3d) peaks.

be noted that Nb-BTESE powder calcined at 500 °C showed the weakest acidity because the pyrolysis of Si-C-Si hybrid silica networks occurred when the calcination temperature reached 500 °C. If we compare NH<sub>3</sub>-TPD result of BTESE 450 powders with that of Nb-BTESE 450 powders, we can find that the peak area under NH<sub>3</sub>-TPD curve for Nb-BTESE 450 powder is much larger than that of BTESE 450. The result indicated that the higher acidity for Nb-BTESE 450 powder was obtained because of the incorporation of Nb dopant [32]. If we analyze the gas permeances of Nb-BTESE membranes, CO<sub>2</sub> sorption data and TPD records of corresponding powders, which are displayed in Figs. 4–6, respectively, evolution for microstructures of Nb-BTESE membranes with the calcination temperature can be proposed as follows. When the calcination temperature was lower than 400 °C, Nb-BTESE membrane showed relatively weak acidity and the density of acidic sites induced by niobium doping was comparatively low. Nb dopant accelerated the densification of pure BTESE membrane, as evidenced by the lower gas permeances of Nb-BTESE membrane calcined at 300 °C in comparison with that of the BTESE membrane calcined at 450 °C. Dominant densification occurred in the Nb-doped hybrid silica networks. Dual effects are working when the heat treat temperature was higher than 400 °C. On the one hand, the increased surface acidity reduced the number of sites and/or affinity for adsorption of CO<sub>2</sub> as the calcination temperature elevated. On the other hand, membrane densification occurred during the calcination process. XPS was used to analyze the surface composition of the Nb-BTESE membranes. The XPS spectra showed the energy absorption from Si, Nb and O elements, which can be found in Fig. 7. The Nb 3d XPS spectrum suggested that the sample produced a single symmetric 3d<sub>5/2</sub> component which, on the basis of its binding energy (207.0 eV), can be assigned to Nb (V) [33]. The results agreed with previously reported binding energy data for Nb<sub>2</sub>O<sub>5</sub> and SiO<sub>2</sub> supported Nb<sub>2</sub>O<sub>5</sub> catalyst [34], which also indicated the presence of Nb<sup>5+</sup> sites in the Nb-doped silica materials. Fig. 8 shows the resulting O 1s photoelectron peak of the Nb-BTESE membrane. It can be seen that the O 1s peak was not symmetrical and can be deconvoluted into two peaks (531.2 eV and 529.7 eV for Si-O and O-Nb, respectively), which suggested the presence of Nb-O-Si linkage [35].

It is widely accepted that pure silica has neither Brönsted nor Lewis acidity. The strong interaction between Nb and hybrid silica networks leads to generation of new acid (Lewis and Brönsted) sites [36]. Several models have been proposed to illustrate the gen-

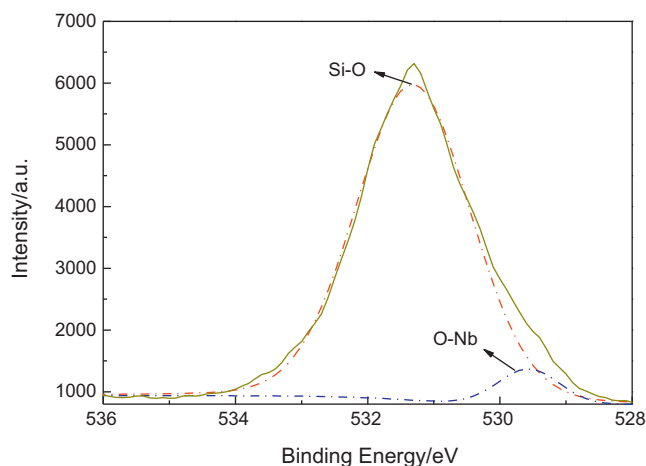


**Fig. 8.** X-ray photoelectron spectrum of the O 1s region for Nb-BTESE powder, which is fitted with a Gaussian distribution (dashed line: fitted peaks).

eration of Lewis and Brönsted acid sites [37]. The Lewis acid sites are caused by coordinative unsaturated Nb atom, while the Brönsted acidity is associated with the presence of Nb-O-Si bridges. Protons are required to compensate the imbalance charge of the oxygen in Nb-O-Si band, and therefore the Brönsted acidity is generated. Burke and Ko [38] reported that the Lewis acid is the main acid between Lewis and Brönsted acid sites. Additionally, Lewis to Brönsted acid sites (L/B ratio) increased as the treatment temperature elevated. It is well-known that the calcination process can promote transformation of Brönsted acid sites to Lewis acid sites. In the present study, we proposed that Lewis acid site, rather than Brönsted acid site, was the dominant factor during the calcination process. A large number of hydroxyl groups on Nb-BTESE membrane surface were lost with the formation of H<sub>2</sub>O molecule during the calcination process, and thereby the Lewis acidity was generated. The more Lewis acid sites of Nb-BTESE membrane might be generated as the calcination temperature elevated, which reduced the net absorption of CO<sub>2</sub> by altering density and strength of the acidic surface centers on the Nb-doped hybrid silica membranes.

#### 4. Conclusions

Niobium modified hybrid silica membranes exhibiting excellent H<sub>2</sub>/CO<sub>2</sub> separation performances and high enough hydrothermal stability, were fabricated using sol-gel method. The observed excellent H<sub>2</sub>/CO<sub>2</sub> permselectivity is due to the incorporation of Nb into hybrid silica networks, therefore creates new Lewis and Brönsted acid sites. Effect of the calcination temperature on H<sub>2</sub>/CO<sub>2</sub> separation properties of Nb-BTESE membrane was investigated in detail.

When the calcination temperature was lower than 400 °C, Nb-BTESE membrane showed relatively weak acidity and the density of acidic sites induced by niobium doping was comparatively low. Dominant densification occurs in the Nb-doped hybrid silica networks. Nb dopant accelerated the densification of pure BTESE membrane, as evidenced by the lower gas permeances of Nb-BTESE membrane calcined at 300 °C in comparison with that of the BTESE membrane calcined at 450 °C. Dual effects are working when the heat treat temperature was higher than 400 °C. On the one hand, the increased surface acidity reduced the number of sites and/or affinity for adsorption of CO<sub>2</sub> as the calcination temperature elevated. On the other hand, membrane densification occurred during the calcination process. Therefore, the permselectivity of H<sub>2</sub>/CO<sub>2</sub> and (He)/CO<sub>2</sub> for Nb-BTESE membrane could be tuned by altering the calcination temperature.

The Nb–BTESE membrane calcined at 450 °C showed both relative high hydrogen permeance ( $\sim 9.7 \times 10^{-8} \text{ mol m}^{-2} \text{ s}^{-1} \text{ Pa}^{-1}$ ) and excellent  $\text{H}_2/\text{CO}_2$  permselectivity (220), as compared with Nb–BTESE membranes calcined at other temperatures.

## Acknowledgements

The authors acknowledge Dr. H. J. M. Bouwmeester (Inorganic Membranes Group, University of Twente, the Netherlands) for his helpful comments and suggestions. The authors also would like to thank the financial support from the **National Natural Science Foundation of China (20906047)**, State Key Laboratory of Chemical Engineering (No. SKL-ChE-09A01), the Natural Science Research Plan of Jiangsu Universities (11KJB530006) and State Key Laboratory of Materials-Oriented Chemical Engineering (No. ZK201002).

## References

- [1] R.M. de Vos, H. Verweij, High-selectivity, high-flux silica membranes for gas separation, *Science* 279 (1998) 1710–1711.
- [2] R.M. de Vos, H. Verweij, Improved performance of silica membranes for gas separation, *J. Membr. Sci.* 143 (1998) 37–51.
- [3] C.-Y. Tsai, S.-Y. Tam, Y. Lu, C.J. Brinker, Dual-layer asymmetric microporous silica membranes, *J. Membr. Sci.* 169 (2000) 255–268.
- [4] Y. Gu, S.T. Oyama, High molecular permeance in a poreless ceramic membrane, *Adv. Mater.* 19 (2007) 1636–1640.
- [5] M.W.J. Luiten, N.E. Benes, C. Huijskes, H. Kruidhof, A. Nijmeijer, Robust method for micro-porous silica membrane fabrication, *J. Membr. Sci.* 348 (2010) 1–5.
- [6] S. Gopalakrishnan, J.C.D. da Costa, Hydrogen gas mixture separation by CVD silica membrane, *J. Membr. Sci.* 323 (2008) 144–147.
- [7] D. Uhlmann, S. Liu, B.P. Ladewig, J.C.D. da Costa, Cobalt-doped silica membranes for gas separation, *J. Membr. Sci.* 326 (2009) 316–321.
- [8] V. Boffa, J.E. ten Elshof, A.V. Petukhov, D.H.A. Blank, Microporous niobia-silica membrane with very low  $\text{CO}_2$  permeability, *ChemSusChem* 1 (2008) 437–443.
- [9] S. Battersby, T. Tasaki, S. Smart, B. Ladewig, S. Liu, M.C. Duke, V. Rudolph, J.C.D. da Costa, Performance of cobalt silica membranes in gas mixture separation, *J. Membr. Sci.* 329 (2009) 91–98.
- [10] Y. Gu, P. Hacarlioglu, S.T. Oyama, Hydrothermally stable silica-alumina composite membranes for hydrogen separation, *J. Membr. Sci.* 310 (2008) 28–37.
- [11] M. Kanezashi, M. Sano, T. Yoshioka, T. Tsuru, Extremely thin Pd-silica mixed-matrix membranes with nano-dispersion for improved hydrogen permeability, *Chem. Commun.* 46 (2010) 6171–6173.
- [12] T. Tsuru, Nano/subnano-tuning of porous ceramic membranes for molecular separation, *J. Sol-Gel Sci. Technol.* 46 (2008) 349–361.
- [13] C. Barboiu, B. Sala, S. Bec, S. Pavan, E. Petit, P. Colomban, J. Sanchez, S. de Perthuis, D. Hittner, Structural and mechanical characterizations of microporous silica-boron membranes for gas separation, *J. Membr. Sci.* 326 (2009) 514–525.
- [14] M. Kanezashi, K. Yada, T. Yoshioka, T. Tsuru, Organic-inorganic hybrid silica membranes with controlled silica network size: preparation and gas permeation characteristics, *J. Membr. Sci.* 348 (2010) 310–318.
- [15] Q. Wei, F. Wang, Z.R. Nie, C.L. Song, Y.L. Wang, Q.Y. Li, Highly hydrothermally stable microporous silica membranes for hydrogen separation, *J. Phys. Chem. B* 112 (2008) 9354–9359.
- [16] H. Qi, J. Han, N.P. Xu, H.J.M. Bouwmeester, Hybrid organic-inorganic microporous membranes with high hydrothermal stability for the separation of carbon dioxide, *ChemSusChem* 3 (2010) 1375–1378.
- [17] M.-T. Tran, N.S. Gnep, G. Szabo, M. Guisnet, Influence of the calcination temperature on the acidic and catalytic properties of sulphated zirconia, *Appl. Catal. A-Gen.* 171 (1998) 207–217.
- [18] Y. Li, S. Yan, W. Yang, Z. Xie, Q. Chen, B. Yue, H. He, Effect of calcination temperature on structure and properties of Sn-Nb<sub>2</sub>O<sub>5</sub>/α-Al<sub>2</sub>O<sub>3</sub> catalyst for ethylene oxide hydration, *Catal. Lett.* 124 (2008) 85–90.
- [19] T. Peters, N. Benes, A. Holmen, J. Keurentjes, Comparison of commercial solid acid catalysts for the esterification of acetic acid with butanol, *Appl. Catal. A-Gen.* 297 (2006) 182–188.
- [20] M.S.P. Francisco, Y. Gushikem, Synthesis and characterization of SiO<sub>2</sub>-Nb<sub>2</sub>O<sub>5</sub> systems prepared by the sol-gel method: structural stability studies, *J. Mater. Chem.* 12 (2002) 2552–2558.
- [21] E.B. Pereira, M.M. Pereira, Y.L. Lam, C.A.C. Perez, M. Schmal, Synthesis and characterization of niobium oxide layers on silica and the interaction with nickel, *Appl. Catal. A-Gen.* 197 (2000) 99–106.
- [22] M. Barczak, A. Dabrowski, J. Ryzczkowski, S. Pasieczna-Patkowska, FT-IR/PAS studies of ethylene-bridged polysiloxanes-quinoxanes functionalized with different groups, *Eur. Phys. J.-Spec. Top.* 154 (2008) 301–304.
- [23] H.L. Castricum, A. Sah, R. Kreiter, D.H.A. Blank, J.F. Vente, J.E. ten Elshof, Hydrothermally stable molecular separation membranes from organically linked silica, *J. Mater. Chem.* 18 (2008) 2150–2158.
- [24] R.M. de Vos, W.F. Maier, H. Verweij, Hydrophobic silica membranes for gas separation, *J. Membr. Sci.* 158 (1999) 277–288.
- [25] S.K. Medda, D. Kundu, G. De, Inorganic-organic hybrid coatings on polycarbonate. Spectroscopic studies on the simultaneous polymerizations of methacrylate and silica networks, *J. Non-Cryst. Solids* 318 (2003) 149–156.
- [26] Y.-H. Han, A. Taylor, M.D. Mantle, K.M. Knowles, Sol-gel-derived organic-inorganic hybrid materials, *J. Non-Cryst. Solids* 353 (2007) 313–320.
- [27] Y. Yan, Y. Hoshino, Z. Duan, S.R. Chaudhuri, A. Sarkar, Design and characterization of interconnected microporous hybrid thin films by a sol-gel process, *Chem. Mater.* 9 (1997) 2583–2587.
- [28] C.-K. Chan, S.-L. Peng, I.-M. Chua, S.-C. Ni, Effects of heat treatment on the properties of poly(methyl methacrylate)/silica hybrid materials prepared by sol-gel process, *Polymer* 42 (2001) 4189–4196.
- [29] M. Kanezashi, A. Yamamoto, T. Yoshioka, T. Tsuru, Characteristics of ammonia permeation through porous silica membranes, *AIChE J.* 56 (2010) 1204–1212.
- [30] Y.H. Ikuhara, H. Mori, T. Saito, Y. Iwamoto, High-temperature hydrogen adsorption properties of precursor-derived nickel nanoparticle-dispersed amorphous silica, *J. Am. Ceram. Soc.* 90 (2007) 546–552.
- [31] H.L. Castricum, R. Kreiter, H.M. van Veen, D.H.A. Blank, J.F. Vente, J.E. ten Elshof, High-performance hybrid pervaporation membranes with superior hydrothermal and acid stability, *J. Membr. Sci.* 324 (2008) 111–118.
- [32] M. Turco, P. Ciambelli, G. Bagnasco, A. La Ginestra, P. Galli, C. Ferragina, TPD study of NH<sub>3</sub> adsorbed by different phases of zirconium phosphate, *J. Catal.* 117 (1989) 355–361.
- [33] L. Dragone, P. Moggi, G. Predieri, R. Zaroni, Niobia and silica-niobia catalysts from sol-gel synthesis: an X-ray photoelectron spectroscopic characterization, *Appl. Surf. Sci.* 187 (2002) 82–88.
- [34] L. Zhang, J.Y. Ying, Synthesis and characterization of mesoporous niobium-doped silica molecular sieves, *AIChE J.* 43 (1997) 2793–2801.
- [35] P. Carniti, A. Gervasini, M. Marzo, Dispersed NbO<sub>x</sub> catalytic phases in silica matrices: influence of niobium concentration and preparative route, *J. Phys. Chem. C* 112 (2008) 14064–14074.
- [36] S. Damyanova, L. Dimitrov, L. Petrov, P. Grange, Effect of niobium on the surface properties of Nb<sub>2</sub>O<sub>5</sub>-SiO<sub>2</sub>-supported Mo catalysts, *Appl. Surf. Sci.* 214 (2003) 68–74.
- [37] X. Gao, I.E. Wachs, Titania-silica as catalysts: molecular structural characteristics and physico-chemical properties, *Catal. Today* 51 (1999) 233–254.
- [38] P.A. Burke, E.I. Ko, Acidic properties of oxides containing niobia on silica and niobia in silica, *J. Catal.* 129 (1991) 38–46.